Publ. Astron. Soc. Japan (2019) 71 (2), 45 (1–12)
doi: 10.1093/pasj/psz016
Advance Access Publication Date: 2019 March 13

A spectroscopic study of weak metallic emission lines in a B3 V star ι Herculis

Kozo SADAKANE[1,*] and Masayoshi NISHIMURA[2]

[1]Astronomical Institute, Osaka Kyoiku University, Asahigaoka, Kashiwara-shi, Osaka 582-8582, Japan
[2]2-6, Nishiyama-Maruo, Yawata-shi, Kyoto 614-8353, Japan

*E-mail: sadakane@cc.osaka-kyoiku.ac.jp

Received 2018 December 10; Accepted 2019 February 5

Abstract

We present a list of weak emission lines (WELs) observed in a sharp-lined B3 V star ι Her (HD 160762) using high-resolution ($R = 65000$) and high-S/N ($\sim$1300) spectral data. The list covers a spectral region between 4900 Å and 10000 Å. We registered 207 WELs in this star and identified 190 lines including ten ions (nine elements). Emission lines of C II, N I, Cr II, Mn II, and Ni II have been identified among normal B-type stars for the first time. Seventeen emission lines remain unidentified. We compared our list with the published list of WELs for 3 Cen A (Wahlgren & Hubrig, 2004, A&A, 418, 1073) and found that the numbers of detected emission lines reflect differences in abundance between these two stars. We detected 13 C I emission lines in ι Her (normal in C), while only one C I emission line was found in 3 Cen A (deficient in C). Many emission lines of P II and Cu II have been detected in 3 Cen A (over-abundant in both P and Cu), while no emission line of these ions has been found in ι Her. Many emission lines of Fe II are visible in the shorter-wavelength side of 6000 Å in ι Her, while these emission lines are missing in 3 Cen A. Close inspections of spectral data of 3 Cen A reveal that the apparently missing Fe II lines appear as absorption lines in this star. Because these two stars have nearly the same atmospheric parameters ($T_{\rm eff}$ and $\log g$), a physical interpretation that is independent of these two parameters is needed to account for this observation.

Key words: stars: atmosphere — stars: early type — stars: individual (ι Herculis (HD 160762))

1 Introduction

The presence of sharp and weak emission lines (WELs) in optical region spectra of B-type stars was initially reported by Sigut, Landstreet, and Shorlin (2000) in a ^{3}He star 3 Cen A (HD 120709). They found sharp emission lines of Mn II, P II, and Hg II ions in the red spectral region. They also found very weak emission lines of Mn II in a mild HgMn star 46 Aql (HD 186122, B9 III). Wahlgren and Hubrig (2000) reported detections of weak emission lines originating from high excitation states of Ti II, Cr II, and Mn II in late B-type HgMn stars. They showed that emission lines of Mn II are absent in HgMn stars for which the Mn enhancement is greater than 1.3 dex and suggested a dependence of the strength of emission lines on the element abundance. Wahlgren and Hubrig (2004) published a list of nearly 350 emission lines of 3 Cen A observed in optical and near-IR spectral regions and identified many emission lines of P II, Mn II, Fe II, Ni II, and Cu II. Since then, WELs have been reported mainly among B-type chemically peculiar stars. Castelli and Hubrig (2004) reported many emission lines of Ti II and Cr II and two emission lines of C I at 8335.15 Å and 9405.72 Å in the HgMn star HD 175640 (B9 V). According to their analysis covering λλ from 3040 Å to

10000 Å, emission lines are selectively found for high excitation lines having large transition probabilities ($\log gf > -1.0$) and these emission lines are found in the red part ($\lambda > 5850$ Å) of the spectrum. Castelli and Hubrig (2007) listed WELs of Cr II, Mn II, and Fe II in a Bp star HR 6000 (HD 144667). Time-variable emission lines of Si II, Mn II, and Fe II were reported in a magnetic Bp star a Cen (HD 125823) by Hubrig and González (2007). Weak emission components of C I, Ti II, Cr II, and Mn II in the HgMn star HD 71066 and those of multiplet 13 lines of Mn II in the PGa star HD 19400 were suggested by Yüce, Castelli, and Hubrig (2011) and by Hubrig et al. (2014), respectively.

Sadakane and Nishimura (2017) presented observations of WELs of Si II and Al II near 6240 Å in many early B-type stars. They demonstrated that the WEL phenomenon is not an exceptional case observed only among chemically peculiar stars but generally observed in many *normal* stars.

Sigut (2001a, 2001b) analyzed WELs of Mn II observed in 3 Cen A and 46 Aql, and showed that these emission lines can be explained by interlocked nonlocal thermodynamic equilibrium (NLTE) effects combined with the presence of vertical stratification. Alternatively, Wahlgren and Hubrig (2000, 2004) discussed a mechanism that the population of highly excited states might be caused by excitation from the far-UV continuum radiation in hot stars. Wahlgren (2008) noted that the NLTE effect can be a significant mechanism for the production of WELs. Sigut and Lester (1996) carried out NLTE radiative transfer calculations of near-IR-region WELs of the Mg II ion in A- and B-type stars and published predictions of line profiles of four Mg II lines between 1.01 μm and 4.76 μm.

Recently, Alexeeva, Ryabchikova, and Mashonkina (2016) and Sitnova, Mashonkina, and Ryabchikova (2018a) constructed comprehensive model atoms for C I and C II and for Ca I and Ca II, respectively, and computed the NLTE line formations for these ions. Alexeeva, Ryabchikova, and Mashonkina (2016) analyzed profiles of four C I lines (8335.15 Å, 9078.28 Å, 9088.51 Å, and 9405.72 Å) and two C II lines (3918.96 Å and 5143.49 Å) observed in ι Her and found that the emission lines of C I and absorption lines of C II were reproduced well by their NLTE calculations. Sitnova, Mashonkina, and Ryabchikova (2018b) demonstrated that profiles of four emission lines of Ca II (6456.88 Å, 8912.07 Å, 8927.36 Å, and 9890.63 Å) observed in ι Her could be reproduced by their NLTE calculations. Sitnova et al. (2018a) found some emission lines of Fe II in the near-IR spectrum of ι Her. They suggested that overionization of the Fe II ion may result in weakened Fe II lines and noted that these lines will either disappear or come into emission in the case of highly excited lines.

Sitnova, Mashonkina, and Ryabchikova (2016) constructed a model atom for Ti I and Ti II, and performed NLTE line formation calculations for these ions. Their target stars were A- to K-type stars, including metal-poor stars with [Fe/H] down to −2.6 dex. Alexeeva et al. (2018) carried out NLTE line formation calculations for Mg I and Mg II lines for B-A-F-G-K stars. They predicted emission lines of Mg I in the infrared region for F-G-K stars.

Since the pioneering work of Wahlgren and Hubrig (2004) on the ^{3}He star 3 Cen A, no list of WELs in an early B-type star has been published. The phenomenon of WELs is observed not only in chemically peculiar stars but also among normal early-type stars. Thus, comprehensive lists of emission lines for representative stars of several spectral types are needed in order to improve the theoretical understanding of the formation mechanism of emission lines. Our primary goal in the present study is to provide a comprehensive list of WELs of as many elements as possible for the bright and sharp-lined normal B3 V star ι Her based on high-quality observational data. We will compare our list with that of 3 Cen A (Wahlgren & Hubrig 2004) and discuss some differences between these two stars. We expect the list to be used as a reference guide and hope to be compared with results of theoretical studies in the future.

2 Observational data

Spectral data of four stars [ι Her, 3 Cen A, γ Peg (HD 886), and 21 Peg (HD 209459)] in the visible to near-IR spectral ranges were obtained with the Echelle Spectro Polarimetric Device for the Observation of Stars (ESPaDOnS)[1] attached to the 3.6 m telescope of the Canada-France-Hawaii Telescope (CFHT) observatory located on the summit of Mauna Kea, Hawaii. Observations with this spectrograph cover the region from 3690 to 10480 Å, and we have used data from 3855 Å to 9980 Å in the present study. Calibrated intensity spectral data were extracted from the ESPaDOnS archive through the Canadian Astronomical Data Centre (CADC). The resolving power is $R = 65000$. Details of the observational data used in the present study are summarized in table 1. For ι Her, we used data observed on two nights (2010 July 20 and 2012 June 25). After averaging downloaded spectral data of each star, we converted the wavelength scale of spectral data of each star into the laboratory scale using measured wavelengths of five He I lines (4471.48 Å, 4713.15 Å, 4921.93 Å, 5015.68 Å, and 5875.62 Å). Errors in the wavelength measurements are around ± 3 km s^{-1} or smaller. Re-fittings of the continuum level of each spectral order were carried out using polynomial functions. The signal-to-noise ratios (S/N) have been

[1] ⟨http://www.cfht.hawaii.edu/Instruments/Spectroscopy/Espadons/⟩.

Table 1. Summary of observational data.

Object	Obs date	Exposure (s)	Number of images
ι Her	2010 July 20	75	20
	2012 June 25	60	50
3 Cen A	2005 May 19	300	2
γ Peg	2008 December 17	20	4
21 Peg	2013 August 17	290	4
	2013 August 23	290	4

Table 2. Signal-to-noise ratio of used data.

Wavelength (Å)	ι Her*	ι Her†	3 Cen A	γ Peg	21 Peg
3900	400	380	230	330	440
4500	1300	1050	550	800	980
5000	1200	1100	770	930	1150
5500	1500	1250	700	1100	1320
6000	850	750	700	680	930
6500	820	880	540	710	950
7000	650	780	510	570	1050
7500	680	640	710	670	1130
8000	700	500	530	680	920
8500	630	900	270	480	700
9000	550	610	380	550	630
9500	510	820	250	350	600
9900	380	720	145	220	470

*Observation date: 2010 July 20.
†Observation date: 2012 June 25.

measured at 13 points from 3900 Å to 9900 Å, using several line-free windows within ±20 Å of the specified wavelength, and the results are given in table 2. In the red and near-IR spectral regions, the S/N ratios are somewhat uncertain because of crowding of telluric absorption lines. We found that the S/N ratios of our data peak in the blue-visible region from ∼4500 Å to ∼5500 Å.

3 The line list

We picked up and registered WELs observed in ι Her in the wavelength region from 3900 Å to 9980 Å. We registered an emission feature only when the feature was seen at the same position for data observed on both nights (2010 July 20 and 2012 June 25). In this way we can avoid possible contaminations from the sky emission. Measurements of the central wavelength and peak intensity of an emission line were done on two nights' data. The emission equivalent width was measured by directly integrating the profile over the local continuum. When an emission line was located in the wing of a strong absorption line, we used the profile of the wing as the local continuum. In such a case, the measured peak intensities sometimes became smaller than 1.0.

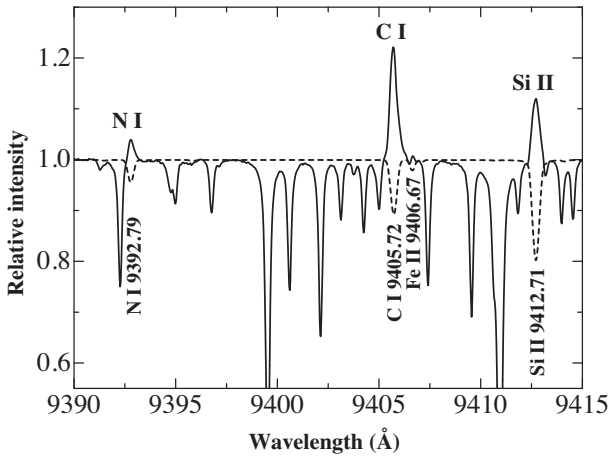

Fig. 1. Sample spectrum of ι Her near 9400 Å. In addition to the strong emission line of C I at 9405.72 Å, emission lines of N I at 9392.79 Å and Si II at 9412.7 Å can be confirmed. The Si II line is actually a blend of two Si II lines, at 9412.67 Å and 9412.78 Å. The solid and dashed lines show observed and simulated spectra, respectively.

The results of two measurements of a line were averaged and then registered.

Line identifications were done with the help of a synthesized spectrum of ι Her using a program developed by Takeda (1995) under the assumption of LTE. Atomic data given in the vald3 database (Ryabchikova et al. 2015) were used in the present study. We adopted atmospheric parameters of ι Her ($T_{\rm eff} = 17500$ K and $\log g = 3.80$) from Nieva and Przybilla (2012), and used an interpolated ATLAS9 model atmosphere (Kurucz 1993) in this study. Data of solar abundances given by Asplund et al. (2009) were used in spectral simulations.

Figure 1 shows an example spectrum between 9390 Å and 9415 Å, where strong telluric absorption lines are overlapping on the stellar spectrum. The dashed line shows a synthesized spectrum. We expect three absorption lines in this region on the simulation. They are N I at 9392.79 Å, C I at 9405.72 Å, and Si II at 9412.67 Å and 9412.78 Å (blended). These three lines are clearly seen in emission in ι Her. The C I 9405.72 Å line in this star has been analyzed by Alexeeva, Ryabchikova, and Mashonkina (2016). A very weak emission feature is observed at 9406.7 Å and this might be attributed to an Fe II line at 9406.67 Å. However, this line is not registered because the line is too close to the neighboring C I line. Figure 2 shows another region near 9900 Å. Spectra of three stars (γ Peg, ι Her, and 3 Cen A) are compared. Two clear emission lines of Ca II at 9890.63 Å and C II at 9903.46 Å can be seen in both γ Peg and ι Her. The emission line of C II at 9903.46 Å has never been reported in stellar spectra. The Ca II line in ι Her has been analyzed by Sitnova, Mashonkina, and Ryabchikova (2018b). In the spectrum of 3 Cen A, emission lines of P II and Mn II are observed (Wahlgren & Hubrig 2004).

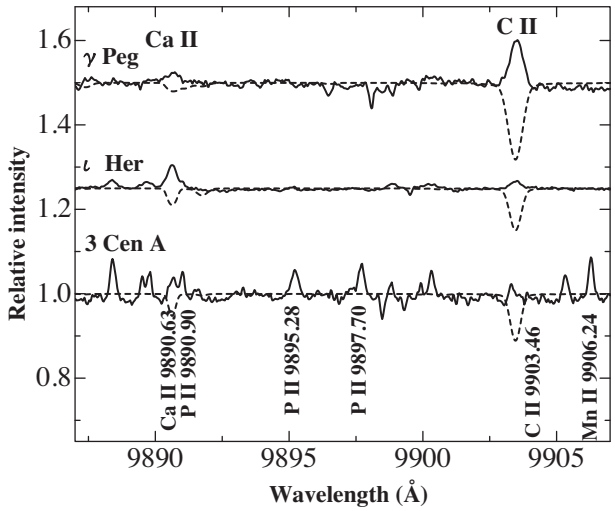

Fig. 2. Sample spectrum of ι Her near 9900 Å. Data of γ Peg and 3 Cen A are shown for comparison. Emission lines of Ca II at 9890.63 Å and C II 9903.46 Å are visible in the two normal stars. The solid and dashed lines show observed and simulated spectra, respectively.

Tables 3 and 4 list 190 identified emission lines in ι Her (hereafter referred to as table 3). Observed wavelengths, peak intensities, and emission equivalent widths together with relevant physical quantities (laboratory wavelengths, log *gf* values, potentials, and configurations) are given. Data of physical quantities have been adopted from the vald3 database. We note that 15 emission lines have two or more candidates for identification (multiple entries).

There are 17 unidentified emission lines which can be seen on two data of the star observed on different nights. We list the measured wavelengths, peak intensities, and emission equivalent widths of these unidentified lines in table 5. Consulting the line list of 3 Cen A prepared by Wahlgren and Hubrig (2004), we find that two entries in table 5 have been given possible identifications within ±0.05 Å of the observed line centers. For example, the feature observed at 8731.72 Å could be identified as an Mn II line at 8731.692 Å, if we follow Wahlgren and Hubrig (2004). We simulated the spectrum of ι Her around 8730 Å using atomic data given in the vald3 database and using the abundance of Mn in this star (Golriz and Landstreet 2017) to find no significant line can be expected at 8731.7 Å. We found a similar result for the line at 8838.33 Å, too. Thus, we leave these two lines in the table of unidentified lines. We further notice that there are 13 common entries of unidentified lines in table 5 and the list of emission lines in 3 Cen A prepared by Wahlgren and Hubrig (2004).

4 Discussion

Our survey of WELs in ι Her resulted in a list of 190 identified lines of 10 ions. We compare in table 6 the numbers of detected emission lines in ι Her and in 3 Cen A. The relative abundances of elements with respect to the Sun in both stars are also shown in the table. 3 Cen A has nearly the same atmospheric parameters ($T_{\rm eff}$ = 17500 K and log g = 3.8; Castelli et al. 1997) as those of ι Her.

We detected in ι Her emission lines of six ions (C II, N I, Cr II, Mn II, and Ni II), which have not been reported earlier for this star. The C II emission line at 9903.46 Å has not been reported for any star. As illustrated in figure 2, the C II emission line is strong in a B2 IV star γ Peg. The emission line is weak but definitely present in ι Her. Although emission lines of N I have been reported in a few chemically peculiar stars such as 3 Cen A (Wahlgren & Hubrig 2004), our detection of three emission lines of N I is the first case among normal stars (figure 1). We found several clear emission lines of Si II in ι Her. Two emission lines of Si II at 5688.82 Å and at 6239.61Å reported by Sadakane and Nishimura (2017) are weak. The newly recorded pair of Si II emission lines at 7848.82 Å and at 7849.72 Å (figure 3) are strong and undisturbed by other lines. These two lines are good candidates to be used in quantitative analyses.

Emission lines of Mn II between 6120 Å and 6135 Å have been reported in many CP stars (e.g., Sigut et al. 2000; Wahlgren & Hubrig 2000), but have not been detected in normal stars. Figure 4 shows a comparison of spectra of ι Her and 3 Cen A in the region between 6118 Å and 6135 Å. We can see three weak emission features (indicated by arrows) in ι Her just at the positions of three Mn II lines at 6122.45 Å, 6128.73 Å, and at 6130.79 Å. Because these emission features are visible on data from two nights (observed on 2010 July 20 and 2012 June 25) and the S/N ratios are higher than ∼750 for both data, we conclude positive detections of three emission lines of Mn II in this star.

Over 130 emission lines of Fe II have been listed in table 3. They all originate from highly excited states of Fe II. We noticed an interesting feature when comparing emission lines of Fe II in ι Her with those observed in the hotter star γ Peg ($T_{\rm eff}$ = 22000 K; Nieva & Przybilla 2012). Figure 5 compares Fe II features between 5502 Å and 5512 Å. There are seven relatively strong lines of Fe II, labeled 1 to 7, all of which arise from highly excited states (near 10.5 eV), in this region. Four lines, labeled 2, 3, 5, and 7, have been registered as emission lines in table 3. The peak intensities of the remaining three lines in ι Her are too weak to be recognized as emission lines. We noticed that line 4 at 5506.20 Å (the line has the largest log *gf* value among the seven lines) shows no emission component but looks nearly filled-in. The line appears as a clear emission line in the hotter star γ Peg. All the other six lines also appear as weaker emission lines in γ Peg. On the other hand, these seven Fe II lines appear as absorption lines in a cooler star 21 Peg

Table 3. Weak emission lines in ι Her: element arrangement.

Ion	λ (Obs) (Å)	Peak int.	E.W. (mÅ)	λ (Lab) (Å)	log *gf*	E_{low} (cm^{-1})	E_{up} (cm^{-1})	Configurations	
C I	4932.08	1.002	0.6	4932.049	−1.658	61981.820	82251.710	2s2.2p.3s 1P*	2s2.2p.4p 1S
C I	5052.16	1.006	1.4	5052.144	−1.303	61981.818	81769.876	2s2.2p.3s 1P*	2s2.2p.4p 1D
C I	7115.19	1.002	1.0	7115.170	−0.934	69710.660	83761.260	2s2.2p.3p 3D	2s2.2p.4d 3F*
C I	7116.99	1.002	0.4	7116.981	−0.907	69744.034	83791.063	2s2.2p.3p 3D	2s2.2p.4d 3F*
C I	8335.16	1.044	17.2	8335.147	−0.437	61981.818	73975.911	2s2.2p.3s 1P*	2s2.2p.3p 1S
C I	9061.46	1.027	10.1	9061.430	−0.347	60352.630	71385.380	2s2.2p.3s 3P*	2s2.2p.3p 3P
C I	9062.49	0.999	11.3	9062.470	−0.455	60333.430	71364.900	2s2.2p.3s 3P*	2s2.2p.3p 3P
C I	9078.30	1.034	13.5	9078.280	−0.581	60352.630	71364.900	2s2.2p.3s 3P*	2s2.2p.3p 3P
C I	9088.55	1.05	13.0	9088.509	−0.430	60352.639	71352.525	2s2.2p.3s 3P*	2s2.2p.3p 3P
C I	9094.88	1.088	29.2	9094.829	0.151	60393.148	71385.390	2s2.2p.3s 3P*	2s2.2p.3p 3P
C I	9111.83	1.041	20.4	9111.799	−0.297	60393.148	71364.918	2s2.2p.3s 3P*	2s2.2p.3p 3P
C I	9405.76	1.229	82.1	9405.724	0.286	61981.818	72610.726	2s2.2p.3s 1P*	2s2.2p.3p 1D
C I	9658.43	1.04	8.9	9658.434	−0.280	60393.148	70743.954	2s2.2p.3s 3P*	2s2.2p.3p 3S
C II	9903.47	0.99	10.0	9903.463	1.021	168978.340	179073.050	2s2.4f 2F*	2s2.5g 2G
N I	8567.79	1.012	1.3	8567.735	−0.670	86137.350	97805.840	2s2.2p2.(3P).3s 2P	2s2.2p2.(3P).3p 2P*
N I	8629.26	1.038	12.1	8629.235	0.077	86220.510	97805.840	2s2.2p2.(3P).3s 2P	2s2.2p2.(3P).3p 2P*
N I	9392.84	1.068	22.4	9392.793	0.300	86220.510	96864.050	2s2.2p2.(3P).3s 2P	2s2.2p2.(3P).3p 2D*
Al II	6231.61	1.018	0.8	6231.621	−0.080	105441.500	121484.252	3s.4p 3P*	3s.4d 3D
				6231.750	0.400	105441.500	121483.920	3s.4p 3P*	3s.4d 3D
Al II	6837.11	1.008	2.1	6837.128	0.080	105470.930	120092.919	3s.4p 3P*	3s.5s 3S
Al II	6920.30	1.008	2.4	6920.343	−0.160	106920.560	121366.725	3s.4p 1P*	3s.5s 1S
Si II	5688.79	1.006	1.0	5688.817	0.110	114414.580	131988.050	3s.3p.(3P*).3d4F*	3s.3p.(3P*).4p4D
Si II	5701.34	1.006	0.4	5701.370	−0.080	114327.150	131861.930	3s.3p.(3P*).3d4F*	3s.3p.(3P*).4p4D
Si II	6239.62	1.028	9.1	6239.614	0.185	103556.030	119578.230	3s2.(1S).4f 2F*	3s2.(1S).6g 2G
				6239.665	0.072	103556.160	119578.230	3s2.(1S).4f 2F*	3s2.(1S).6g 2G
Si II	6818.46	1.005	1.2	6818.414	−0.565	103860.740	118522.860	3s2.(1S).5p 2P*	3s2.(1S).6d 2D
Si II	6829.83	1.011	3.0	6829.799	−0.311	103885.250	118522.930	3s2.(1S).5p 2P*	3s2.(1S).6d 2D
Si II	7125.92	1.002	0.3	7125.848	−0.809	103885.250	117914.800	3s2.(1S).5p 2P*	3s2.(1S).7s 2S
Si II	7848.81	1.038	11.1	7848.816	0.316	101023.050	113760.320	3s2.(1S).4d 2D	3s2.(1S).5f 2F*
Si II	7849.71	1.044	13.2	7849.722	0.470	101024.350	113760.150	3s2.(1S).4d 2D	3s2.(1S).5f 2F*
Si II	7911.57	1.005	2.4	7911.520	−0.464	113760.150	126396.470	3s2.(1S).5f 2F*	3s2.(1S).9g 2G
				7911.626	−0.577	113760.320	126396.470	3s2.(1S).5f 2F*	3s2.(1S).9g 2G
Si II	8044.47	1.007	2.8	8044.407	−0.722	112394.560	124822.140	3s2.(1S).5d 2D	3s2.(1S).8f 2F*
				8044.549	−0.567	112394.720	124822.080	3s2.(1S).5d 2D	3s2.(1S).8f 2F*
Si II	8935.53	1.008	7.2	8935.495	−0.158	113760.150	124948.400	3s2.(1S).5f 2F*	3s2.(1S).8g 2G
				8935.631	−0.271	113760.320	124948.400	3s2.(1S).5f 2F*	3s2.(1S).8g 2G
Si II	9412.71	1.141	27.4	9412.665	1.012	103556.030	114177.100	3s2.(1S).4f 2F*	3s2.(1S).5g 2G
				9412.780	0.899	103556.160	114177.100	3s2.(1S).4f 2F*	3s2.(1S).5g 2G
Ca II	6456.86	1.009	2.1	6456.875	0.155	68056.910	83540.000	3p6.(1S).4f 2F*	3p6.(1S).6g 2G
Ca II	8133.08	1.012	4.2	8133.097	−0.475	78034.390	90326.450	3p6.(1S).5f 2F*	3p6.(1S).9g 2G
Ca II	8201.78	1.009	2.5	8201.722	0.343	60533.020	72722.230	3p6.(1S).5p 2P*	3p6.(1S).5d 2D
Ca II	8248.84	1.015	3.0	8248.796	0.556	60611.280	72730.930	3p6.(1S).5p 2P*	3p6.(1S).5d 2D
Ca II	8254.86	1.008	1.8	8254.720	−0.398	60611.280	72722.230	3p6.(1S).5p 2P*	3p6.(1S).5d 2D
Ca II	8912.08	1.034	13.4	8912.068	0.637	56839.250	68056.910	3p6.(1S).4d 2D	3p6.(1S).4f 2F*
Ca II	8927.43	1.029	9.8	8927.356	0.811	56858.460	68056.910	3p6.(1S).4d 2D	3p6.(1S).4f 2F*
Ca II	9890.66	1.026	18.1	9890.628	1.013	68056.910	78164.720	3p6.(1S).4f 2F*	3p6.(1S).5g 2G
Cr II	8784.35	1.001	4.6	8784.409	−0.728	82763.750	94144.430	3d4.(5D).5s e6D	3d4.(5D).5p 6P*
Cr II	8839.00	0.992	3.7	8838.915	−1.211	82692.060	94002.560	3d4.(5D).5s e6D	3d4.(5D).5p 6P*
Mn II	6122.44	1.009	1.3	6122.450	0.955	82136.400	98465.210	3d5.(6S).4d e5D	3d5.(6S).4f 5F*
Mn II	6128.81	1.004	0.4	6128.733	0.594	82151.160	98463.230	3d5.(6S).4d e5D	3d5.(6S).4f 5F*
Mn II	6130.77	1.004	0.3	6130.801	0.359	82155.840	98462.410	3d5.(6S).4d e5D	3d5.(6S).4f 5F*
Fe II	4948.78	1.006	0.8	4948.791	−0.031	83459.721	103661.038	3d6.(5D).4d e6F	3d6.(5D<2>).4f 2[2]*
Fe II	5061.67	1.005	0.6	5061.710	0.284	83136.508	102887.172	3d6.(5D).4d e6F	3d6.(5D<4>).4f 2[4]*

Table 3. (Continued)

Ion	λ (Obs) (Å)	Peak int.	E.W. (mÅ)	λ (Lab) (Å)	log *gf*	E_{low} (cm^{-1})	E_{up} (cm^{-1})	Configurations	
Fe II	5067.90	1.006	1.4	5067.890	−0.078	83308.241	103034.819	3d6.(5D).4d e6F	3d6.(5D<4>).4f 2[2]*
Fe II	5075.72	1.005	1.0	5075.760	0.184	84326.967	104022.961	3d6.(5D).4d 6P	3d6.(5D<0>).4f 2[3]*
Fe II	5089.20	1.010	1.7	5089.213	0.013	83308.241	102952.170	3d6.(5D).4d e6F	3d6.(5D<4>).4f 2[3]*
Fe II	5117.03	1.005	0.7	5117.031	−0.039	84131.624	103668.762	3d6.(5D).4d 6D	3d6.(5D<2>).4f 2[1]*
Fe II	5144.31	1.007	1.3	5144.352	0.307	84424.422	103857.804	3d6.(5D).4d 6P	3d6.(5D<1>).4f 2[2]*
Fe II	5148.90	1.005	0.9	5148.898	−0.417	83990.106	103406.327	3d6.(5D).4d 6D	3d6.(5D<3>).4f 2[2]*
				5149.004	−0.036	105211.079	124626.900	3d6.(5D).5d 4G	3d6.(3F<3>).4f 2[5]*
Fe II	5180.31	1.013	2.2	5180.312	−0.088	83812.352	103110.835	3d6.(5D).4d 6D	3d6.(5D<4>).4f 2[1]*
Fe II	5194.87	1.006	0.7	5194.886	−0.108	84424.422	103668.762	3d6.(5D).4d 6P	3d6.(5D<2>).4f 2[1]*
Fe II	5203.63	1.007	0.8	5203.634	−0.115	83812.352	103024.341	3d6.(5D).4d 6D	3d6.(5D<4>).4f 2[2]*
Fe II	5210.56	1.008	1.4	5210.550	0.793	103165.320	122351.810	3d6.(3P).4d 4F	3d6.(3P<2>).4f 2[5]*
Fe II	5216.81	1.008	0.7	5216.858	0.478	84710.749	103874.040	3d6.(5D).4d e6G	3d6.(5D<1>).4f 2[4]*
				5216.859	0.670	84527.806	103691.094	3d6.(5D).4d e6G	3d6.(5D<2>).4f 2[5]*
Fe II	5223.28	1.007	0.9	5223.256	−0.169	83812.352	102952.170	3d6.(5D).4d 6D	3d6.(5D<4>).4f 2[3]*
Fe II	5247.94	1.017	2.7	5247.956	0.550	84938.265	103988.001	3d6.(5D).4d e6G	3d6.(5D<1>).4f 2[3]*
Fe II	5251.20	1.010	0.9	5251.226	0.424	84844.866	103882.740	3d6.(5D).4d e6G	3d6.(5D<1>).4f 2[4]*
Fe II	5262.34	1.005	0.8	5262.313	−0.368	85048.655	104046.419	3d6.(5D).4d f4D	3d6.(5D<0>).4f 2[3]*
Fe II	5306.18	1.008	1.6	5306.182	0.044	84870.911	103711.610	3d6.(5D).4d f4D	3d6.(5D<2>).4f 2[4]*
Fe II	5347.22	1.010	1.7	5347.188	−0.268	85172.826	103869.046	3d6.(5D).4d f4D	3d6.(5D<1>).4f 2[2]*
Fe II	5429.97	1.011	1.1	5429.987	0.427	85462.907	103874.040	3d6.(5D).4d e4G	3d6.(5D<1>).4f 2[4]*
Fe II	5442.38	1.005	0.3	5442.359	−0.313	85048.655	103417.935	3d6.(5D).4d f4D	3d6.(5D<3>).4f 2[1]*
Fe II	5445.82	1.009	1.8	5445.800	−0.109	85048.655	103406.327	3d6.(5D).4d f4D	3d6.(5D<3>).4f 2[2]*
Fe II	5457.71	1.007	1.4	5457.722	−0.138	85728.846	104046.419	3d6.(5D).4d 4S	3d6.(5D<0>).4f 2[3]*
Fe II	5465.93	1.015	2.5	5465.932	0.348	85679.755	103969.814	3d6.(5D).4d e4G	3d6.(5D<1>).4f 2[3]*
Fe II	5487.61	1.005	0.2	5487.618	0.288	85462.907	103680.689	3d6.(5D).4d e4G	3d6.(5D<2>).4f 2[4]*
Fe II	5492.07	1.005	0.6	5492.079	0.091	85679.755	103882.740	3d6.(5D).4d e4G	3d6.(5D<1>).4f 2[4]*
Fe II	5492.42	1.004	0.4	5492.398	−0.097	84685.245	102887.172	3d6.(5D).4d f4D	3d6.(5D<4>).4f 2[4]*
Fe II	5493.80	1.007	0.7	5493.831	0.259	84685.245	102882.424	3d6.(5D).4d f4D	3d6.(5D<4>).4f 2[4]*
Fe II	5503.22	1.005	0.4	5503.215	−0.120	84685.245	102851.394	3d6.(5D).4d f4D	3d6.(5D<4>).4f 2[5]*
Fe II	5503.89	1.006	0.6	5503.894	−0.725	84870.911	103034.819	3d6.(5D).4d f4D	3d6.(5D<4>).4f 2[2]*
Fe II	5507.07	1.009	1.5	5507.071	−0.056	84870.911	103024.341	3d6.(5D).4d f4D	3d6.(5D<4>).4f 2[2]*
Fe II	5511.10	1.007	1.4	5511.087	−0.378	85728.846	103869.046	3d6.(5D).4d 4S	3d6.(5D<1>).4f 2[2]*
Fe II	5529.06	1.012	2.2	5529.053	−0.258	84870.911	102952.170	3d6.(5D).4d f4D	3d6.(5D<4>).4f 2[3]*
Fe II	5532.09	1.005	0.9	5532.086	−0.099	84870.911	102942.256	3d6.(5D).4d f4D	3d6.(5D<4>).4f 2[3]*
Fe II	5549.01	1.008	1.3	5549.000	−0.186	84870.911	102887.172	3d6.(5D).4d f4D	3d6.(5D<4>).4f 2[4]*
Fe II	5558.30	1.005	0.6	5558.286	−0.781	85048.655	103034.819	3d6.(5D).4d f4D	3d6.(5D<4>).4f 2[2]*
Fe II	5577.95	1.005	0.8	5577.912	−0.106	85462.907	103385.785	3d6.(5D).4d e4G	3d6.(5D<3>).4f 2[3]*
Fe II	5588.19	1.005	0.3	5588.221	0.163	85462.907	103352.723	3d6.(5D).4d e4G	3d6.(5D<3>).4f 2[5]*
Fe II	5746.56	1.005	0.7	5746.566	−0.402	85728.846	103125.717	3d6.(5D).4d 4S	3d6.(5D<4>).4f 2[1]*
Fe II	5783.61	1.008	0.8	5783.623	0.365	86416.370	103701.778	3d6.(5D).4d e4F	3d6.(5D<2>).4f 2[5]*
Fe II	5784.46	1.008	1.0	5784.445	0.145	86599.791	103882.740	3d6.(5D).4d e4F	3d6.(5D<1>).4f 2[4]*
Fe II	5842.30	1.005	0.7	5842.294	−0.328	86599.791	103711.610	3d6.(5D).4d e4F	3d6.(5D<2>).4f 2[4]*
Fe II	5854.21	1.005	0.9	5854.187	−0.113	86599.791	103676.848	3d6.(5D).4d e4F	3d6.(5D<2>).4f 2[3]*
Fe II	5885.03	1.016	3.2	5885.014	0.298	86710.911	103698.515	3d6.(5D).4d e4F	3d6.(5D<2>).4f 2[3]*
Fe II	5902.83	1.008	1.2	5902.823	0.416	86416.370	103352.723	3d6.(5D).4d e4F	3d6.(5D<3>).4f 2[5]*
Fe II	5955.71	1.016	3.5	5955.698	0.252	86599.791	103385.785	3d6.(5D).4d e4F	3d6.(5D<3>).4f 2[3]*
Fe II	6172.61	1.005	1.2	6172.627	−1.721	77861.650	94057.727	3d6.(5D).5s e6D	3d5.(4D).4s.4p.(3P*) 6D*
Fe II	6291.84	1.020	4.2	6291.826	0.348	88157.176	104046.419	3d6.(5D).4d 4P	3d6.(5D<0>).4f 2[3]*
Fe II	6357.22	1.010	1.6	6357.161	0.235	87985.667	103711.610	3d6.(5D).4d 4P	3d6.(5D<2>).4f 2[4]*
Fe II	6375.80	1.011	2.2	6375.796	−0.011	88189.066	103869.046	3d6.(5D).4d 4P	3d6.(5D<1>).4f 2[2]*
Fe II	6455.21	1.007	1.2	6455.153	−0.350	88189.066	103676.286	3d6.(5D).4d 4P	3d6.(5D<2>).4f 2[1]*
Fe II	6491.67	1.005	1.2	6491.663	−0.046	87985.667	103385.785	3d6.(5D).4d 4P	3d6.(5D<3>).4f 2[3]*
Fe II	6548.40	0.985	0.9:	6548.391	−0.415	88853.535	104120.244	3d6.(5D).5p 6D*	3d6.(5D).5d 6P
Fe II	7409.05	1.008	1.5	7409.053	−1.362	78525.442	92018.727	3d6.(5D).5s e6D	3d5.(4D).4s.4p.(3P*) 6F*

Table 3. (Continued)

Ion	λ (Obs) (Å)	Peak int.	E.W. (mÅ)	λ (Lab) (Å)	log *gf*	E_{low} (cm^{-1})	E_{up} (cm^{-1})	Configurations	
Fe II	7495.66	1.012	2.3	7495.627	−0.004	78237.709	91575.149	3d6.(5D).5s e6D	3d6.(5D).5p w6P*
Fe II	7506.57	1.018	4.3	7506.544	−0.425	78525.442	91843.485	3d6.(5D).5s e6D	3d6.(3P1).4p 6P*
Fe II	7513.22	1.041	10.8	7513.176	0.294	77861.650	91167.936	3d6.(5D).5s e6D	3d6.(5D).5p w6P*
Fe II	7516.23	1.013	2.6	7516.185	0.104	98294.909	111595.869	3d6.(3H).5s e4H	3d6.(3H).5p 4H*
Fe II	7520.80	1.006	1.2	7520.739	−1.529	78725.822	92018.727	3d6.(5D).5s e6D	3d5.(4D).4s.4p.(3P*) 6F*
Fe II	7574.05	1.011	2.2	7574.024	−0.074	98445.410	111644.798	3d6.(3H).5s e4H	3d5.(4G)4s.4p(1P*)
Fe II	7579.43	1.099	1.8	7579.322	−1.063	78725.790	91915.950	3d6.(5D).5s e6D	3d5.(4D).4s.4p.(3P) 6F*
				7579.559	−1.132	78725.822	91915.570	3d6.(5D).5s e6D	3d5.(4D).4s.4p.(3P*) 6F*
Fe II	7592.70	1.006	1.7	7592.685	−0.095	98568.907	111735.854	3d6.(3H).5s e4H	3d6.(3F).5p 4H*
Fe II	7731.72	1.016	3.9	7731.688	−0.108	78237.709	91167.936	3d6.(5D).5s e6D	3d6.(5D).5p w6P*
Fe II	7755.59	1.015	3.3	7755.571	−0.587	79439.496	92329.905	3d6.(5D).5s e4D	3d5.(4G).4s.4p.(3P*) v4F*
Fe II	7789.33	1.013	2.8	7789.279	−0.641	79439.496	92274.123	3d6.(5D).5s e4D	3d6.(3P1).4p 4P*
Fe II	8057.54	1.008	1.7	8057.498	−0.083	99824.051	112231.439	3d6.(3F2).5s f4F	3d6.(3G).5p 4F*
Fe II	8064.29	1.003	0.9	8064.284	−0.957	79885.523	92282.470	3d6.(5D).5s e4D	3d5.(4G).4s.4p.(3P*) v4F*
Fe II	8069.73	1.005	0.7	8069.718	−0.619	79885.523	92274.123	3d6.(5D).5s e4D	3d6.(3P1).4p 4P*
Fe II	8072.41	1.005	1.0	8072.386	−0.321	99688.355	112072.860	3d6.(3F2).5s f4F	3d6.(3F).5p 4G*
Fe II	8082.40	1.019	6.0	8082.385	0.199	99688.355	112057.539	3d6.(3F2).5s f4F	3d6.(3F).5p 4G*
Fe II	8101.46	1.014	1.4	8101.483	−0.344	79885.523	92225.549	3d6.(5D).5s e4D	3d6.(5D).5p 4P*
Fe II	8118.94	1.005	0.4	8118.891	0.313	99573.244	111886.812	3d6.(3F2).5s f4F	3d6.(3F).5p 4G*
Fe II	8137.20	1.018	4.3	8137.181	0.543	102584.984	114870.874	3d6.(3G).5s f4G	3d6.(3G).5p 4G*
Fe II	8157.63	1.004	2.1	8157.571	−0.412	78525.442	90780.623	3d6.(5D).5s e6D	3d6.(5D).5p 4F*
Fe II	8237.17	1.014	3.9	8237.168	−0.568	80178.005	92314.764	3d6.(5D).5s e4D	3d6.(5D).5p 4P*
Fe II	8287.88	1.031	7.8	8287.877	0.749	77861.650	89924.150	3d6.(5D).5s e6D	3d6.(5D).5p 6F*
Fe II	8298.16	1.015	3.5	8298.166	−0.289	80178.005	92225.549	3d6.(5D).5s e4D	3d6.(5D).5p 4P*
Fe II	8301.57	1.028	5.5	8301.527	0.415	97507.414	109550.081	3d6.(3p).5s 4P	3d6.(3P).5p 4D*
Fe II	8352.83	1.011	2.7	8352.828	−0.389	80346.060	92314.764	3d6.(5D).5s e4D	3d6.(5D).5p 4P*
Fe II	8420.59	1.010	2.6	8420.561	−0.059	78525.442	90397.873	3d6.(5D).5s e6D	3d6.(5D).5p 4D*
Fe II	8423.95	1.026	5.6	8423.925	−0.010†	78725.822	90593.511	3d6.(5D).5s e6D	3d6.(5D).5p 6F*
Fe II	8451.04	1.034	10.5	8451.015	−0.290	78237.709	90067.357	3d6.(5D).5s e6D	3d6.(5D).5p 6F*
Fe II	8468.61	1.000	6.0	8468.592	0.315	78237.709	90042.804	3d6.(5D).5s e6D	3d6.(3F1).4p 4G*
Fe II	8469.27	0.990	5.4	8469.235	−0.146	78844.031	90648.230	3d6.(5D).5s e6D	3d6.(5D).5p 6F*
Fe II	8490.13	1.045	15.1	8490.102	0.181	78525.442	90300.628	3d6.(5D).5s e6D	3d6.(5D).5p 6F*
Fe II	8490.72	0.998	2.5	8490.691	0.504	89924.150	101698.519	3d6.(5D).5p 6F*	3d6.(5D).6s 6D
Fe II	8499.64	0.985	9.2	8499.616	0.169	78725.822	90487.827	3d6.(5D).5s e6D	3d6.(5D).5p 6F*
Fe II	8508.72	0.981	2.2	8508.677	−0.219†	78844.031	90593.511	3d6.(5D).5s e6D	3d6.(5D).5p 6F*
Fe II	8570.80	1.006	0.8	8570.835	−0.406	98130.136	109794.406	3d6.(3H).5s e4H	3d6.(3H).5p 4I*
Fe II	8636.63	1.052	14.6	8636.581	0.704	99093.452	110668.928	3d6.(3H).5s e2H	3d6.(3H).5p 2H*
				8636.539	−2.184	93129.879	104705.411	3d6.(3F1).4p 4D*	3d6.(5D).5d 4D
Fe II	8678.61	0.960	4.8	8678.563	0.747	102584.984	114104.465	3d6.(3G).5s f4G	3d6.(3G).5p 4H*
				8678.570	−2.652	60445.279	71964.750	3d5.4s2 c4D	3d6.(3D).4p 4P*
Fe II	8722.46	1.011	6.1	8722.461	0.868	98130.136	109591.643	3d6.(3H).5s e4H	3d6.(3H).5p 4I*
				8722.364	−0.215	79439.496	90901.130	3d6.(5D).5s e4D	3d6.(5D).5p 4P*
Fe II	8732.77	0.965	3.5	8732.746	−0.080	98568.907	110016.915	3d6.(3H).5s e4H	3d6.(3H).5p 4G*
				8732.823	−1.424	100492.025	111939.932	3d6.(3F2).5s e2F	3d5.(4G)4s.4p(1P*)4F*
Fe II	8774.66	0.976	4.5	8774.633	0.292	103172.173	114565.532	3d6.(3G).5s 4G	3d6.(3G).5p 4H*
Fe II	8792.09	0.997	2.1	8792.079	−0.145	99573.244	110943.996	3d6.(3F2).5s f4F	3d6.(3H).5p 2H*
Fe II	8809.00	1.011	2.1	8808.933	0.146	98445.410	109794.406	3d6.(3H).5s e4H	3d6.(3H).5p 4I*
Fe II	8813.38	1.024	5.9	8813.371	0.095	98568.907	109912.188	3d6.(3H).5s e4H	3d6.(3F).5p 4G*
Fe II	8814.55	1.014	5.1	8814.519	0.043	98114.577	109456.381	3d6.(3P).5s 4P	3d6.(3P).5p 4P*
Fe II	8827.80	1.016	3.4	8827.758	0.715	98294.909	109619.704	3d6.(3H).5s e4H	3d6.(3H).5p 4I*
Fe II	8833.99	1.014	8.6	8833.972	0.543	98445.410	109762.239	3d6.(3H).5s e4H	3d6.(3H).5p 4I*
Fe II	8847.08	0.970	3.9	8847.040	0.245	97507.414	108807.527	3d6.(3p).5s 4P	3d6.(3P).5p 4P*

Table 3. (Continued)

Ion	λ (Obs) (Å)	Peak int.	E.W. (mÅ)	λ (Lab) (Å)	log *gf*	E_{low} (cm^{-1})	E_{up} (cm^{-1})	Configurations	
Fe II	8926.72	1.027	10.1	8926.657	0.209	79439.496	90638.823	3d6.(5D).5s e4D	3d6.(5D).5p 4D*
Fe II	9070.49	1.007	1.9	9070.462	−0.377	80178.005	91199.776	3d6.(5D).5s e4D	3d6.(5D).5p 4D*
Fe II	9075.58	1.042	12.9	9075.538	0.151	79885.523	90901.130	3d6.(5D).5s e4D	3d6.(5D).5p 4P*
Fe II	9077.40	1.032	10.2	9077.394	0.069	79885.523	90898.878	3d6.(5D).5s e4D	3d6.(3P1).4p 4P*
Fe II	9122.95	1.052	15.5	9122.935	0.357	79439.496	90397.873	3d6.(5D).5s e4D	3d6.(5D).5p 4D*
Fe II	9132.40	1.052	12.8	9132.385	0.426	79439.496	90386.533	3d6.(5D).5s e4D	3d6.(5D).5p 4F*
Fe II	9159.29	1.025	6.0	9159.271	0.552	99332.102	110247.006	3d6.(3H).5s e2H	3d6.(3H).5p 2I*
Fe II	9166.32	1.027	7.3	9166.302	0.578	103608.921	114515.453	3d6.(3G).5s 2G	3d6.(3G).5p 2H*
Fe II	9175.99	1.027	5.8	9175.920	0.479	79885.523	90780.623	3d6.(5D).5s e4D	3d6.(5D).5p 4F*
Fe II	9178.10	1.047	15.2	9178.058	0.362	80178.005	91070.566	3d6.(5D).5s e4D	3d6.(5D).5p 4F*
Fe II	9179.50	1.035	7.2	9179.492	0.128	78237.709	89128.569	3d6.(5D).5s e6D	3d6.(5D).5p 6P*
Fe II	9187.22	1.041	12.3	9187.183	0.242	78237.709	89119.452	3d6.(5D).5s e6D	3d6.(5D).5p 6D*
Fe II	9196.98	1.044	11.1	9196.922	−0.002	80178.005	91048.225	3d6.(5D).5s e4D	3d6.(5D).5p 4D*
Fe II	9201.53	1.008	1.0	9201.489	0.059	97507.414	108372.239	3d6.(3p).5s 4P	3d6.(3P).5p 4S*
Fe II	9203.24	1.041	12.3	9203.177	0.199	80346.060	91208.892	3d6.(5D).5s e4D	3d6.(5D).5p 4F*
Fe II	9204.13	1.034	5.1	9204.095	0.608	77861.650	88723.398	3d6.(5D).5s e6D	3d6.(5D).5p 6D*
Fe II	9210.92	0.975	2.6	9210.907	−0.348	80346.060	91199.776	3d6.(5D).5s e4D	3d6.(5D).5p 4D*
Fe II	9507.73	1.021	9.2	9507.705	0.449	98294.909	108809.810	3d6.(3H).5s e4H	3d5.(4G).4s.4p.(1P*) 4H*
Fe II	9510.02	1.003	1.6	9510.012	−0.577	79885.523	90397.873	3d6.(5D).5s e4D	3d6.(5D).5p 4D*
Fe II	9655.73	1.021	1.4	9655.696	0.327	98130.136	108483.877	3d6.(3H).5s e4H	3d5.(4G).4s.4p.(1P*)4G*
Fe II	9790.49	1.014	4.5	9790.538	1.160	102840.320	113051.461	3d6.(5D<4>).4f 2[6]*	3d6.(5D<4>).5g 2[7]
Fe II	9792.37	0.990	2.2	9792.404	0.990	102831.393	113040.588	3d6.(5D<4>).4f 2[5]*	3d6.(5D<4>).5g 2[6]
Fe II	9830.57	1.035	9.3	9830.460	0.590	102887.172	113056.847	3d6.(5D<4>).4f 2[4]*	3d6.(5D<4>).5g 2[4]
				9830.499	1.100	103325.974	113495.605	3d6.(5D<3>).4f 2[5]*	3d6.(5D<3>).5g 2[6]
				9830.723	0.340	103326.445	113495.846	3d6.(5D<3>).4f 2[4]*	3d6.(5D<3>).5g 2[4]
Fe II	9833.39	1.018	2.6	9833.406	0.830	103326.445	113493.072	3d6.(5D<3>).4f 2[4]*	3d6.(5D<3>).5g 2[5]
Fe II	9841.53	1.011	8.9	9841.496	0.500	102882.424	113040.688	3d6.(5D<4>).4f 2[4]*	3d6.(5D<4>).5g 2[6]
				9841.587	1.070	102893.426	113051.600	3d6.(5D<4>).4f 2[6]*	3d6.(5D<4>).5g 2[7]
Fe II	9873.79	0.995	3.5	9873.768	0.830	103857.804	113982.872	3d6.(5D<1>).4f 2[2]*	3d6.(5D<1>).5g 2[3]
Fe II	9881.28	1.023	7.4	9881.294	1.070	103874.040	113991.394	3d6.(5D<1>).4f 2[4]*	3d6.(5D<1>).5g 2[5]
Fe II	9898.85	0.970	6.1	9898.837	1.070	103701.778	113801.203	3d6.(5D<2>).4f 2[5]*	3d6.(5D<2>).5g 2[6]
Fe II	9909.16	0.979	5.8	9909.110	1.160	103420.207	113509.161	3d6.(5D<3>).4f 2[6]*	3d6.(5D<3>).5g 2[7]
Fe II	9910.15	0.995	7.5	9910.093	1.220	103421.213	113509.167	3d6.(5D<3>).4f 2[6]*	3d6.(5D<3>).5g 2[7]
Fe II	9926.06	0.976	5.8	9926.059	0.950	104022.961	114094.688	3d6.(5D<0>).4f 2[3]*	3d6.(5D<0>).5g 2[4]
Fe II	9927.54	0.976	8.1	9927.516	1.220	103019.688	113089.937	3d6.(5D<4>).4f 2[7]*	3d6.(5D<4>).5g 2[8]
Fe II	9946.26	0.979	4.0	9946.244	0.950	103969.814	114021.102	3d6.(5D<1>).4f 2[3]*	3d6.(5D<1>).5g 2[4]
Fe II	9947.86	0.979	5.2	9947.838	1.280	103040.370	113090.048	3d6.(5D<4>).4f 2[7]*	3d6.(5D<4>).5g 2[8]
Ni II	8096.70	1.010	3.1	8096.749	0.710	91800.050	104147.290	3p6.3d8.(3F).5s 4F	3p6.3d8.(3F).5p 4G*
Ni II	8106.29	1.008	1.6	8106.263	0.374	93528.440	105861.190	3p6.3d8.(3F).5s 2F	3p6.3d8.(3F).5p 2D*
Ni II	8121.46	1.006	0.4	8121.494	0.508	93528.440	105838.060	3p6.3d8.(3F).5s 2F	3p6.3d8.(3F).5p 2F*
Ni II	8126.46	1.005	1.3	8126.419	0.199	94067.140	106369.300	3p6.3d8.(3F).5s 4F	3p6.3d8.(3F).5p 4F*
Ni II	8140.48	1.006	1.5	8140.428	0.366	91800.050	104081.040	3p6.3d8.(3F).5s 4F	3p6.3d8.(3F).5p 2G*
Ni II	8141.91	1.011	1.5	8141.933	0.380	93390.060	105668.780	3p6.3d8.(3F).5s 4F	3p6.3d8.(3F).5p 4F*
Ni II	8183.73	1.007	1.0	8183.722	0.386	94067.140	106283.160	3p6.3d8.(3F).5s 4F	3p6.3d8.(3F).5p 4G*
Ni II	8350.22	1.006	1.0	8350.263	0.330	92325.850	104298.230	3p6.3d8.(3F).5s 4F	3p6.3d8.(3F).5p 4F*
Ni II	8407.22	1.013	1.4	8407.213	0.494	94729.250	106620.530	3p6.3d8.(3F).5s 2F	3p6.3d8.(3F).5p2G*
Ni II	8434.33	1.008	6.8	8434.379	0.504	91800.050	103653.030	3p6.3d8.(3F).5s 4F	3p6.3d8.(3F).5p 4D*

†Taken from the NIST database (Kramida, A., Ralchenko, Yu., Reader, J., & NIST ASD Team, 2018, NIST Atomic Spectra Database, version 5.6.1, ⟨https://doi.org/10.18434/T4W30F⟩).

Table 4. Weak emission lines in ι Her: wavelength arrangement.*

Ion	λ (Obs) (Å)	Peak int.	E.W. (mÅ)	λ (Lab) (Å)	log *gf*	E_{low} (cm^{-1})	E_{up} (cm^{-1})	Configurations	
C I	4932.08	1.002	0.6	4932.049	−1.658	61981.820	82251.710	2s2.2p.3s 1P*	2s2.2p.4p 1S
Fe II	4948.78	1.006	0.8	4948.791	−0.031	83459.721	103661.038	3d6.(5D).4d e6F	3d6.(5D<2>).4f 2[2]*
C I	5052.16	1.006	1.4	5052.144	−1.303	61981.818	81769.876	2s2.2p.3s 1P*	2s2.2p.4p 1D
Fe II	5061.67	1.005	0.6	5061.710	0.284	83136.508	102887.172	3d6.(5D).4d e6F	3d6.(5D<4>).4f 2[4]*
Fe II	5067.90	1.006	1.4	5067.890	−0.078	83308.241	103034.819	3d6.(5D).4d e6F	3d6.(5D<4>).4f 2[2]*
Fe II	5075.72	1.005	1.0	5075.760	0.184	84326.967	104022.961	3d6.(5D).4d 6P	3d6.(5D<0>).4f 2[3]*
Fe II	5089.20	1.010	1.7	5089.213	0.013	83308.241	102952.170	3d6.(5D).4d e6F	3d6.(5D<4>).4f 2[3]*
Fe II	5117.03	1.005	0.7	5117.031	−0.039	84131.624	103668.762	3d6.(5D).4d 6D	3d6.(5D<2>).4f 2[1]*
Fe II	5144.31	1.007	1.3	5144.352	0.307	84424.422	103857.804	3d6.(5D).4d 6P	3d6.(5D<1>).4f 2[2]*

*A complete listing of this table is available as "Supplementary data" in the online version.

Table 5. Unidentified emission lines.

λ (Å)	Peak intensity	E. W. (mÅ)	Note*
6476.60	1.005	0.6	
8129.37	1.010	3.1	unknown
8215.72	1.014	2.6	
8304.26	1.012	2.0	unknown
8459.34	1.000	2.6	unknown
8682.87	0.977	3.1	unknown
8719.69	1.000	1.3	unknown
8731.72	0.960	1.8	Mn II 8731.692
8767.58	0.968	5.0	unknown
8780.16	0.982	2.8	unknown
8788.38	0.993	1.2	unknown
8825.57	1.017	5.4	unknown
8838.33	0.999	5.7	Ti II 8838.415
8882.14	1.000	3.2	
8910.43	1.020	8.0	unknown
8953.90	1.013	5.1	unknown
8961.82	1.016	3.9	

*Entries given in the line list of 3 Cen A (Wahlgren & Hubrig 2004).

Table 6. Number of registered emission lines.

Ion	ι Her		3 Cen A	
	N	[X/H]	N	[X/H]
C I	13	−0.05*	1	−0.75*
C II	1	—	0	—
N I	3	0.03*	3	0.44*
N II	0	—	1	—
Al II	3	0.13*	0	−1.37*
Si II	12	−0.01*	6	−0.15*
P II	0	0.04*	44	2.01*
Ca II	8	−0.02†	3	−0.14‡
Ti II	0	−0.16*	2	0.32*
Cr II	2	−0.07*	4	0.08*
Mn II	3	−0.2†	34	1.60*
Fe II	135	−0.37*	137‖	0.42*
Co II	0	−0.48†	2	—
Ni II	10	−0.27*	30	0.46*
Cu II	0	−1.17†	15	2.00§
Hg II	0	1.95†	1	3.30*

*Sadakane and Nishimura (2018).
†Golriz and Landstreet (2017).
‡Hardorp, Bidelman, and Prölss (1968).
§Castelli, Parthasarathy, and Hack (1997).
‖Nine additional Fe II lines have been detected in 3 Cen A among emission lines noted as unknown in Wahlgren and Hubrig (2004).

($T_{\rm eff} = 10400$ K; Fossati et al. 2009). The equivalent widths of these seven absorption lines of Fe II are in accordance with the LTE simulation for 21 Peg. We guess that ι Her might be a transitional case. When we go from cooler to hotter stars, weak Fe II lines turn into emission at lower temperature and strong lines remain as weak absorption lines in transitional cases. Then strong lines turn into emission at even higher temperatures.

In table 6, we notice a correlation between the number of detected emission lines and the abundances. In the case of C I, we detected 13 emission lines in ι Her, while only one emission line of this ion has been reported in 3 Cen A by Wahlgren and Hubrig (2004). Carbon has a normal abundance in ι Her, while the element is under-abundant in 3 Cen A (Sadakane & Nishimura 2018). This relation can be found in the case of Al II, too. We detected three emission line of Al II in ι Her, in which Al is normal. Wahlgren and Hubrig (2004) listed no emission line of Al II in 3 Cen A, in which Al is definitely under-abundant (Sadakane & Nishimura 2018). Castelli, Parthasarathy, and Hack (1997) showed that P, Mn, and Cu are all over-abundant in 3 Cen A, and Wahlgren and Hubrig (2004) reported many emission lines of P II, Mn II, and Cu II in this star. We detected no emission lines of P II and Cu II and found only three very weak emission lines of Mn II in ι Her. Similar relations can be found for Ti II and Ni II, too. These findings support the suggestion as to the dependence

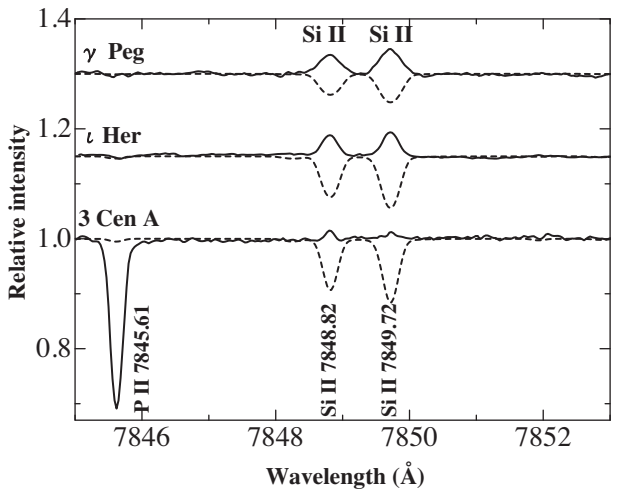

Fig. 3. Sample spectrum of ι Her near a pair of Si II emission lines at 7848.82 Å and at 7849.72 Å. Data for γ Peg and 3 Cen A are shown for comparison. The weakness of these emission lines in 3 Cen A is to be noted, in which the abundance of Si is −0.14 dex lower than that in ι Her. The solid and dashed lines show observed and simulated spectra, respectively.

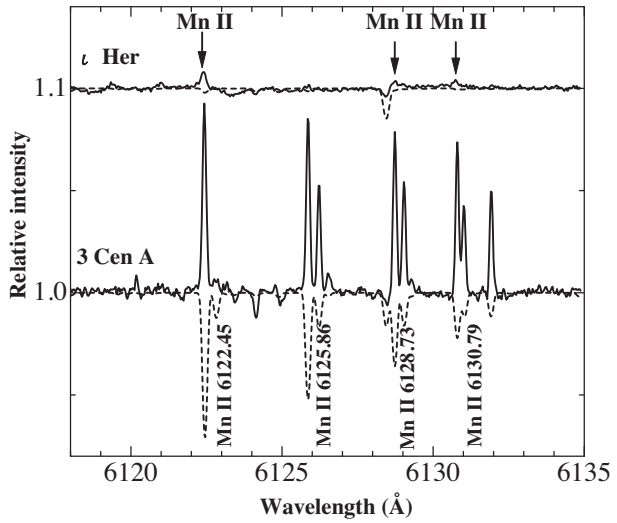

Fig. 4. Emission lines of Mn II in ι Her near 6120 Å. Data of 3 Cen A are shown for comparison. The solid and dashed lines show observed and simulated spectra, respectively. An overabundance of Mn by 1.6 dex was assumed in the simulation for 3 Cen A. We notice three weak emission lines of Mn II in ι Her (indicated by arrows).

of strengths of emission lines on the element abundance (Wahlgren & Hubrig 2000).

We list 46 emission lines of Fe II in the shorter wavelength side of 6000 Å in ι Her. Curiously, however, most of these emission lines are missing in the list of 3 Cen A. Wahlgren and Hubrig (2004) measured only one emission line of Fe II, at 5794.90 Å, between 4900 Å and 6000 Å. The line is not observed in ι Her. They listed the line as an Fe II line at 5794.726 Å or a Si II line at 5794.890 Å. A weak emission line can be seen at 5794.89 Å in our data for 3 Cen A, and

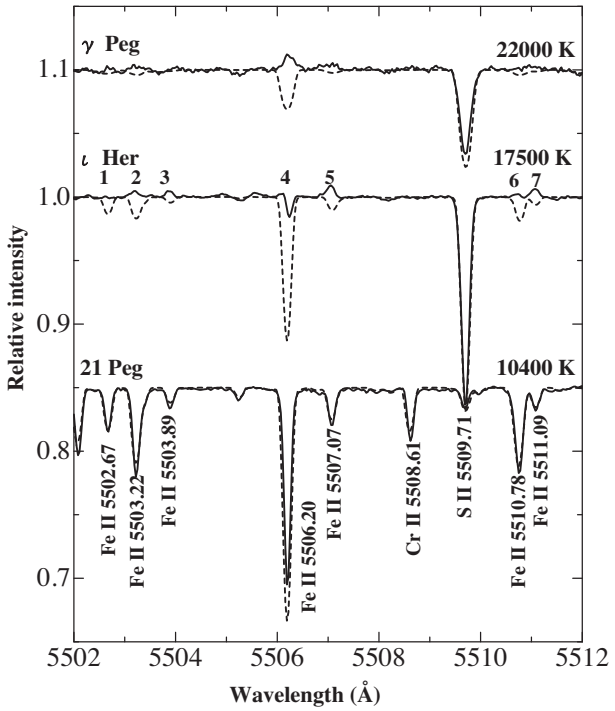

Fig. 5. Weak emission lines of Fe II near 5506 Å. Observed (solid line) and simulated (dashed line) spectra for three stars (γ Peg, ι Her, and 21 Peg) are compared.

we suggest the Si II line at 5794.890 Å as a better candidate because of the coincidence between the observed and laboratory wavelengths. Close inspection of our spectral data for 3 Cen A reveals that most of these apparently missing Fe II lines appear as absorption lines in this star (figure 6, panel A). It is natural that these lines are not included in the list of emission lines. On the contrary, most of the Fe II WELs found in ι Her also appear as emission lines in 3 Cen A on the longer wavelength side of 6000 Å (figure 6, panel B). The measured equivalent widths of the Fe II emission lines in ι Her (taken from table 3) are plotted against the wavelength in figure 7. Those of corresponding lines in 3 Cen A are shown for comparison. We can see an upward trend (from left to right) in the equivalent widths of the Fe II lines of 3 Cen A. This shows that a transition from absorptions to emissions occurs at around 6000 Å. The contrast in the behaviors of Fe II lines on the shorter wavelength side of 6000 Å between ι Her and 3 Cen A might be related to a phenomenon reported by Wahlgren and Hubrig (2000). They found an anti-correlation between the strength of the emission line of Mn II at 6122.43 Å and the Mn abundance enhancement. Among the HgMn stars they observed, stars with large values of [Mn/H] (higher than ∼1.3 dex) do not show emission in this line. The abundance of Fe in 3 Cen A is higher than that in ι Her by at least 0.3 dex (Sadakane & Nishimura 2018), and a similar mechanism may be involved. Because these two stars have nearly the same

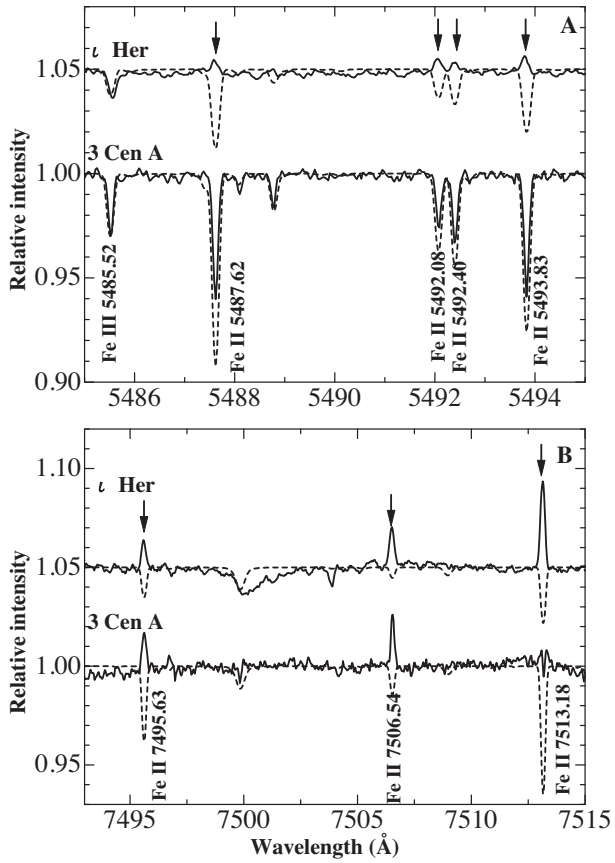

Fig. 6. Comparison of Fe II lines between ι Her and 3 Cen A in two wavelength regions. In the upper panel, Fe II lines appear as absorption in 3 Cen A, while they are in emission in the lower panel. The solid and dashed lines show observed and simulated spectra, respectively. Abundances of Fe obtained by Sadakane and Nishimura (2018) for these two stars have been used in the simulations.

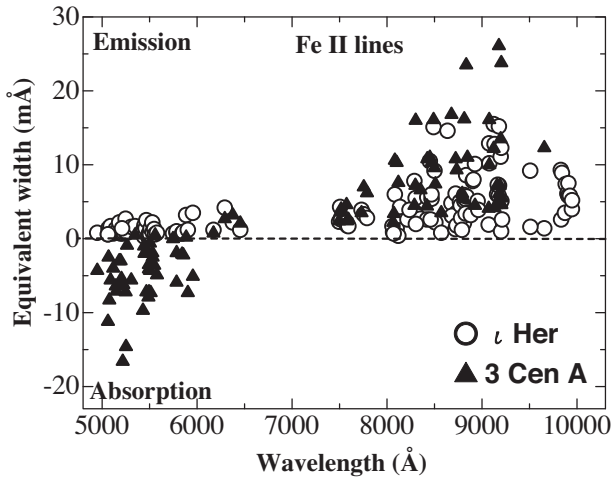

Fig. 7. Equivalent widths of Fe II lines in ι Her (open circles) and in 3 Cen A (filled triangles) plotted against the wavelength. Data for ι Her are taken from table 3. The equivalent widths of corresponding lines in 3 Cen A on the shorter wavelength side of 6000 Å are measured using our own data, while those on the longer wavelength side are taken from Wahlgren and Hubrig (2004). The emission and absorption lines are plotted in the upper (positive) and lower (negative) parts, respectively.

atmospheric parameters ($T_{\rm eff}$ and log g), a physical interpretation independent of these two parameters is needed.

Supplementary data

Supplementary data are available at *PASJ* online.

Complete listing of table 4.

Acknowledgments

This research is based on CFHT public science archive data retrieved through the Canadian Astronomy Data Centre and has made use of the SIMBAD database, operated by CDS, Strasbourg, France. We thank the referee for providing valuable comments which helped to improve the manuscript.

References

Alexeeva, S. A., Ryabchikova, T. A., & Mashonkina, L. I. 2016, MNRAS, 462, 1123
Alexeeva, S., Ryabchikova, T., Mashonkina, L., & Hu, S. 2018, ApJ, 866, 153
Asplund, M., Grevesse, N., Sauval, A. J., & Scott, P. 2009, ARA&A, 47, 481
Castelli, F., & Hubrig, S. 2004, A&A, 425, 263
Castelli, F., & Hubrig, S. 2007, A&A, 475, 1041
Castelli, F., Parthasarathy, M., & Hack, M. 1997, A&A, 321, 254
Fossati, L., Ryabchikova, T., Bagnulo, S., Alecian, E., Grunhut, J., Kochukhov, O., & Wade, G. 2009, A&A, 503, 945
Golriz, S. S., & Landstreet, J. D. 2017, MNRAS, 466, 1597
Hardorp, J., Bidelman, W. P., & Prölss, J. 1968, Z. Astrophys., 69, 429
Hubrig, S., & González, J. F. 2007, A&A, 466, 1083
Hubrig, S., et al. 2014, MNRAS, 442, 3604
Kurucz, R. L. 1993, Kurucz CD-ROM, No. 13, ATLAS9 Stellar Atmosphere Programs and 2 km/s Grid (Cambridge, MA: Harvard-Smithsonian Center for Astrophysics)
Nieva, M.-F., & Przybilla, N. 2012, A&A, 539, A143
Ryabchikova, T., Piskunov, N., Kurucz, R. L., Stempels, H. C., Heiter, U., Pakhomov, Yu., & Barklem, P. S. 2015, Phys. Scripta, 90, 054005
Sadakane, K., & Nishimura, M. 2017, PASJ, 69, 48
Sadakane, K., & Nishimura, M. 2018, PASJ, 70, 40
Sigut, T. A. A. 2001a, ApJ, 546, L115
Sigut, T. A. A. 2001b, A&A, 377, L27
Sigut, T. A. A., Landstreet, J. D., & Shorlin, S. L. S. 2000, ApJ, 530, L89
Sigut, T. A. A., & Lester, J. B. 1996, ApJ, 461, 972
Sitnova, T. M., Mashonkina, L. I., & Ryabchikova, T. A. 2016, MNRAS, 461, 1000
Sitnova, T. M., Mashonkina, L. I., & Ryabchikova, T. A. 2018a, MNRAS, 477, 3343

Sitnova, T., Ryabchikova, T., Alexeeva, S., & Mashonkina, L. 2018b, in IAU Symp. 334, Rediscovering our Galaxy, ed. C. Chiappini et al. (Cambridge: Cambridge University Press), 360
Takeda, Y. 1995, PASJ, 47, 287
Wahlgren, G. M. 2008, Contrib. Astron. Obs. Skalnaté Pleso, 38, 279
Wahlgren, G. M., & Hubrig, S. 2000, A&A, 362, L13
Wahlgren, G. M., & Hubrig, S. 2004, A&A, 418, 1073
Yüce, K., Castelli, F., & Hubrig, S. 2011, A&A, 528, A37